nature medicine

LETTERS

https://doi.org/10.1038/s41591-018-0264-7

Aurora kinase A drives the evolution of resistance to third-generation EGFR inhibitors in lung cancer

Khyati N. Shah[1,2], Roma Bhatt[1,2], Julia Rotow[2,3], Julia Rohrberg[2,3], Victor Olivas[2,3], Victoria E. Wang[2], Golzar Hemmati[2,3], Maria M. Martins[2,3], Ashley Maynard[2,3], Jonathan Kuhn[4], Jacqueline Galeas[2], Hayley J. Donnella[1,2], Swati Kaushik[1,2], Angel Ku[1,2], Sophie Dumont[4], Gregor Krings[5], Henry J. Haringsma[6], Liliane Robillard[6], Andrew D. Simmons[6], Thomas C. Harding[6], Frank McCormick[2], Andrei Goga[2,4], Collin M. Blakely[2,3], Trever G. Bivona[2,3] and Sourav Bandyopadhyay[1,2*]

Although targeted therapies often elicit profound initial patient responses, these effects are transient due to residual disease leading to acquired resistance. How tumors transition between drug responsiveness, tolerance and resistance, especially in the absence of preexisting subclones, remains unclear. In epidermal growth factor receptor (EGFR)-mutant lung adenocarcinoma cells, we demonstrate that residual disease and acquired resistance in response to EGFR inhibitors requires Aurora kinase A (AURKA) activity. Nongenetic resistance through the activation of AURKA by its coactivator TPX2 emerges in response to chronic EGFR inhibition where it mitigates drug-induced apoptosis. Aurora kinase inhibitors suppress this adaptive survival program, increasing the magnitude and duration of EGFR inhibitor response in preclinical models. Treatment-induced activation of AURKA is associated with resistance to EGFR inhibitors in vitro, in vivo and in most individuals with EGFR-mutant lung adenocarcinoma. These findings delineate a molecular path whereby drug resistance emerges from drug-tolerant cells and unveils a synthetic lethal strategy for enhancing responses to EGFR inhibitors by suppressing AURKA-driven residual disease and acquired resistance.

The approval and use of epidermal growth factor receptor (EGFR) inhibitors in *EGFR*-mutant non-small-cell lung cancer (NSCLC) has been a major clinical breakthrough, helping to define the paradigm of precision medicine. However, EGFR tyrosine kinase inhibitors (TKIs) often produce an incomplete response followed by progression and acquired resistance in 9–12 months, often a lethal event[1–3]. Disease progression occurs through tumor evolution on treatment, involving distinct genetic and nongenetic changes in cell state and signaling[4]. Furthermore, patient tumors develop acquired resistance via multiple mechanisms simultaneously[5–8], and this polyclonal nature of resistance could limit the efficacy of approaches that target any single genetic driver of resistance. The heterogeneous nature of acquired resistance highlights the need to better understand and target residual disease, defined as the fraction of tumor cells that survive initial treatment and ultimately enable tumor progression in the presence of ongoing treatment[9]. Acquired resistance occurs through the selection of preexisting clones as well as the evolution of drug-tolerant (that is, persister) cells without genetic alterations that survive treatment through tumor cell adaptation that may involve the acquisition of genetic mutations later[10–12]. Both genetic and nongenetic forms of resistance to EGFR TKIs have been identified, including secondary mutations in EGFR, amplification of various receptor tyrosine kinases, transformation to small-cell lung cancer and epithelial–mesenchymal transition (EMT)[4,13–16]. Third-generation EGFR inhibitors, rociletinib and the US Food and Drug Administration–approved agent osimertinib, bind and inhibit mutant EGFR with and without the T790M mutation associated with resistance to previous-generation EGFR inhibitors[1,2]. For these drugs, approximately half of acquired resistance cases have unknown genetic drivers, and when genetic drivers exist, multiple drivers often co-occur in the same patient[7,8,13]. We identified a synthetic lethal interaction between EGFR TKIs and Aurora kinase inhibitors in acquired resistant cells that has important implications for the development of new treatment strategies aimed at preventing rather than intercepting acquired resistance.

We modeled acquired resistance to both osimertinib and rociletinib by deriving polyclonal acquired resistant cell lines on the basis of stepwise dose escalation over a period of 9 d followed by maintenance in 1 μM of drug over 6 weeks (osimertinib-resistant lines are denoted by OR and rociletinib-resistant lines by RR; see Fig. 1a). We generated eight acquired resistant models from four different EGFR-mutant NSCLC cell lines including PC9, HCC827 and HCC4006 expressing an *EGFR* exon 19 deletion and H1975 expressing a compound *EGFR* L858R and T790M mutation. There was a greater than tenfold change in half maximal inhibitory concentration (IC_{50}) in each line compared to parental cells, and we also observed cross-resistance between drugs indicating a shared mechanism of resistance regardless of which EGFR inhibitor was used (Fig. 1b and Supplementary Fig. 1a). In response to TKI, resistant cells suppressed EGFR signaling, and we observed no activation of alternate receptor tyrosine kinases previously reported to facilitate bypass of EGFR inhibition (Supplementary Fig. 1b)[17]. In response to treatment, resistant cells demonstrated heightened extracellular signal-regulated kinase (ERK) and protein kinase B (PKB/Akt) signaling and reduced apoptosis, as measured by cleaved poly(ADP-ribose) polymerase (PARP), compared to parental cells (Fig. 1c). Exome sequencing revealed no recurrent mutations among independently derived acquired resistant lines, and no additional

[1]Department of Bioengineering and Therapeutic Sciences, University of California, San Francisco, San Francisco, CA, USA. [2]Helen Diller Family Comprehensive Cancer Center, University of California, San Francisco, San Francisco, CA, USA. [3]Department of Medicine, University of California, San Francisco, San Francisco, CA, USA. [4]Department of Cell and Tissue Biology, University of California, San Francisco, San Francisco, CA, USA. [5]Department of Pathology, University of California, San Francisco, San Francisco, CA, USA. [6]Clovis Oncology, Inc., Boulder, CO, USA. *e-mail: sourav.bandyopadhyay@ucsf.edu

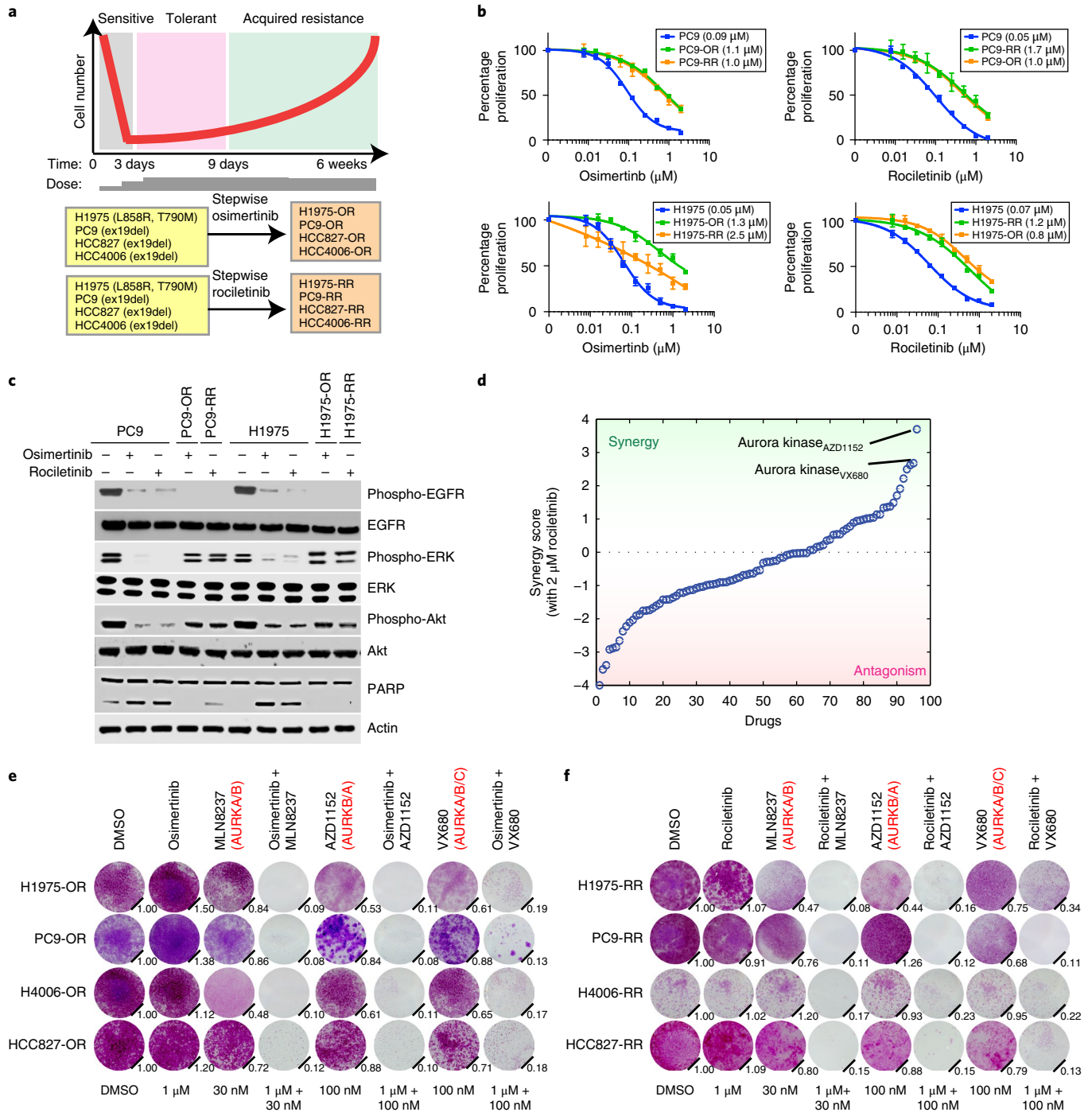

Fig. 1 | EGFR-mutant lung adenocarcinoma cells that demonstrate acquired resistance to third-generation EGFR TKIs are sensitive to Aurora kinase inhibition. a, Schematic of cell numbers throughout the process to generate EGFR-mutant lung adenocarcinoma cell lines with acquired resistance through continuous cell culture and stepwise dose escalation of either osimertinib or rociletinib from 10 nM to 1 μM over the course of 9 d. Cell lines and EGFR mutation are listed. **b**, Mean relative proliferation of parental cell lines and those with acquired resistance to osimertinib (denoted by OR) or rociletinib (denoted by RR) treated with the indicated agents and allowed to proliferate for 3 d. IC_{50} analysis of dose–response curves from $n = 4$ biologically independent samples. The IC_{50} for each cell line is indicated in parentheses. **c**, Immunoblot analysis showing activity of the EGFR, PKB/Akt and ERK as well as PARP cleavage in response to DMSO, osimertinib (1 μM) or rociletinib (1 μM) (+ indicates 24-h treatment, − indicates treatment was not given) in parental or acquired-resistant cell lines. Actin is the loading control. The experiment was performed twice with similar results. **d**, Sorted results from a combination drug screen across 94 drugs combined with 2 μM rociletinib in H1975-RR cells. Synergy is based on enhancement of growth inhibition compared to either drug alone (Methods). Screening was performed once. **e**,**f**, Crystal violet staining of parental and OR (**e**) or RR (**f**) cell lines 9 d after treatment with DMSO or the indicated drugs. Aurora kinase inhibitors are annotated with their relative targets in order of potency. Quantification (relative number of stained cells) is shown on the bottom right. Data in **c**, **e** and **f** are representative of two independent experiments. The error bars are the s.e.m. Full blots are shown in Supplementary Fig. 11.

mutations in EGFR were detected (data not shown). We next sought to identify whether these cells harbored markers of cell states known to be associated with resistance to EGFR TKIs. Compared to parental cells, resistant cells had an increase in vimentin levels indicative of EMT, increased nuclear factor kappa-light-chain-enhancer of activated B cells (NF-κB) signaling and minor changes in cancer cell stemness, all known to be associated with EGFR TKI resistance (Supplementary Fig. 1c)[4,12,17–20]. Tumor protein p53 (TP53) and neuroblastoma RAS viral oncogene homolog (NRAS) signaling were not strongly associated with resistance (Supplementary Fig. 1d,e)[21,22]. Heritability analysis using single-cell clones indicated that the majority of cells derived from acquired resistant lines were resensitized to TKI after a period of drug withdrawal, indicating a nongenetic and reversible mechanism of drug resistance (Supplementary Fig. 1f).

On the basis of the absence of any obviously targetable driver of resistance, we sought to identify pathways revealed by drugs that synergistically inhibit growth when combined with EGFR TKIs. Across a 94-compound cancer-focused library, both Aurora kinase inhibitors in the panel, AZD1152 and VX680, were the top synergistic candidates when combined with 2 μM rociletinib in H1975-RR cells (Fig. 1d and Supplementary Table 1). The combination of these two agents as well as MLN8237, the most clinically advanced Aurora kinase inhibitor, with either osimertinib or rociletinib demonstrated synergistic reduction in cell growth in all models (Fig. 1e,f and Supplementary Fig. 2a,b). Aurora kinase inhibitors display significant cross-reactivity between AURKA, AURKB and AURKC[23]. Therefore, these data reveal a primary requirement for Aurora kinase signaling in models of acquired resistance to third-generation inhibitors of EGFR.

We sought to determine the relevant target of Aurora kinase inhibitors in driving drug synergy. We found approximately twofold messenger RNA upregulation but no increase in total protein levels for all three Aurora kinases in resistant cells compared to parental cells (Fig. 2a and Supplementary Fig. 3a,b). In contrast, we found significant activation of AURKA, but not AURKB or AURKC, in resistant models as indicated by increased autophosphorylation at T288 (Fig. 2a and Supplementary Fig. 3b). We next asked whether activation of AURKA is sufficient to confer resistance to EGFR TKIs. AURKA activity peaks during the G2/M phase of the cell cycle where it regulates chromosome alignment, mitotic spindle formation and chromosome segregation[24]. Parental PC9 cells synchronized using serum starvation or thymidine block into the G2/M phase had high levels of phosphorylated AURKA (phospho-AURKA), were more viable and had diminished apoptosis in comparison to parental cells that were treated when they were in the G1/S phase or asynchronously (Supplementary Fig. 3c–i). Transient AURKA overexpression, but not AURKB, caused resistance to EGFR TKIs at levels comparable to the Kirsten rat sarcoma viral oncogene homolog (KRAS) G12V mutant, a known driver of resistance (Fig. 2b and Supplementary Fig. 3j)[25].

AURKA can be activated by upstream factors that facilitate its autophosphorylation, including targeting protein for Xklp2 (TPX2), neural precursor cell expressed developmentally down-regulated protein 9 (NEDD9), protein ajuba (AJUBA) and serine/threonine-protein kinase PAK 1 (PAK-1)[26]. We investigated each one and observed a consistent increase in TPX2 protein, and to a lesser extent transcription, and an increase in phospho-AURKA in all resistant models (Fig. 2c and Supplementary Fig. 4a,b). TPX2 activates AURKA by locking it in an active conformation and protecting it from protein phosphatases[24]. Overexpression of TPX2 activated AURKA and caused EGFR TKI resistance (Fig. 2b), whereas expression of other reported AURKA activators did not (Supplementary Fig. 4c,d). TPX2 is degraded by the ubiquitin E3 ligase anaphase-promoting complex (APC) bound to the specific activator cadherin-1 (CDH1) during mitotic exit and the G1 phase[27]. Using subcellular fractionation, we confirmed that CDH1 was nuclear in parental and resistant cells as previously reported[28]. In contrast, TPX2 was cytosolic in cells with acquired resistance, whereas in parental cells it was more likely to be nuclear (Supplementary Fig. 4e). Hence, TPX2 is not colocalized with the complex responsible for its degradation in resistant cells. Together, these data suggest that altered TPX2 localization in cells with acquired resistance contributes to AURKA activation during the interphase and promotes acquired resistance to third-generation EGFR TKIs.

We next sought to determine the mechanism of synergy focusing on MLN8237, the most advanced AURKA inhibitor (Fig. 1e,f). Combination treatment resulted in a reduction in cell proliferation and an increase in cell death measured by YO-PRO-1 positivity in models with acquired resistance (Fig. 2d,e). In PC9-RR mouse xenografts, rociletinib partially abrogated tumor growth and led to rapid tumor progression, combination of rociletinib and MLN8237 led to a stronger initial reduction in tumor growth, which was sustained for 70 d ($P = 2.2 \times 10^{-11}$) (Fig. 2f). We observed no apparent toxicity on the basis of body weight (Supplementary Fig. 5a). We observed similar results with osimertinib, which in combination with MLN8237 resulted in decreased tumor growth in nine out of ten tumors derived from PC9-OR cells ($P = 0.001$) (Fig. 2g and Supplementary Fig. 5b). To understand how AURKA might regulate apoptosis and proliferation, we probed several signaling pathways known to be associated with resistance to EGFR inhibitors[18,19,29]. Combination treatment caused a decrease in ERK and NF-κB signaling, indicating multiple potentially overlapping routes through which AURKA signaling contributes to cell growth (Fig. 2h and Supplementary Fig. 6). Therefore, the combination of EGFR and Aurora kinase inhibitors induces apoptosis and acts synergistically in suppressing the growth of acquired resistant cells in vitro and in vivo.

We next sought to understand the molecular mechanisms underlying how this combination engaged the apoptotic machinery, focusing on proapoptotic factor Bcl-2-like protein 11 (BIM) because its induction is essential for cell death induced by EGFR TKIs[30,31]. BIM and its splice variant BIM extra long (BIM-EL) are regulated by phosphorylation leading to proteasomal degradation[32]. EGFR inhibition alone in parental PC9 cells suppressed phospho-BIM, resulting in the accumulation of BIM-EL, and induced PARP cleavage consistent with previous reports (Fig. 2h)[30,31]. In contrast, in resistant cells the combination of EGFR TKI and MLN8237 was necessary to suppress phospho-BIM, leading to the accumulation of BIM-EL, its primary effector apoptosis regulator BAX (BAX) and cleaved PARP (Fig. 2h). In normal cells, AURKA suppresses apoptosis during mitosis by suppressing BIM[24,33]. Since acquired resistant cells expressed high levels of phospho-AURKA throughout the cell cycle in contrast to parental cells (Supplementary Fig. 3d), these data indicate that resistant cells co-opt this natural function of AURKA for use throughout the cell cycle, thereby exploiting a redundancy in the control of BIM that is normally temporally segregated. Therefore, cells with acquired resistance escape from EGFR inhibition through a shift in the control of the proapoptotic machinery from EGFR alone to both EGFR and AURKA (Fig. 2i).

We next sought to elucidate the temporal processes leading to AURKA activation in cells with acquired resistance. On the basis of our modeling after treatment, we divided the period of drug response into three distinct phases: (i) a sensitive phase; (ii) a drug-tolerant phase in which remaining cells persist; and (iii) a proliferative acquired-resistance phase. We measured signaling dynamics across a time course of 9 d in H1975 cells treated with osimertinib and compared this with H1975-OR cells that were exposed for more than 6 weeks (Fig. 3a). While osimertinib treatment inhibited EGFR throughout, we observed BIM-mediated apoptosis for 2 days, after which it was suppressed indicating that the remaining cells were drug-tolerant. In the sensitive phase, we observed a gradual increase

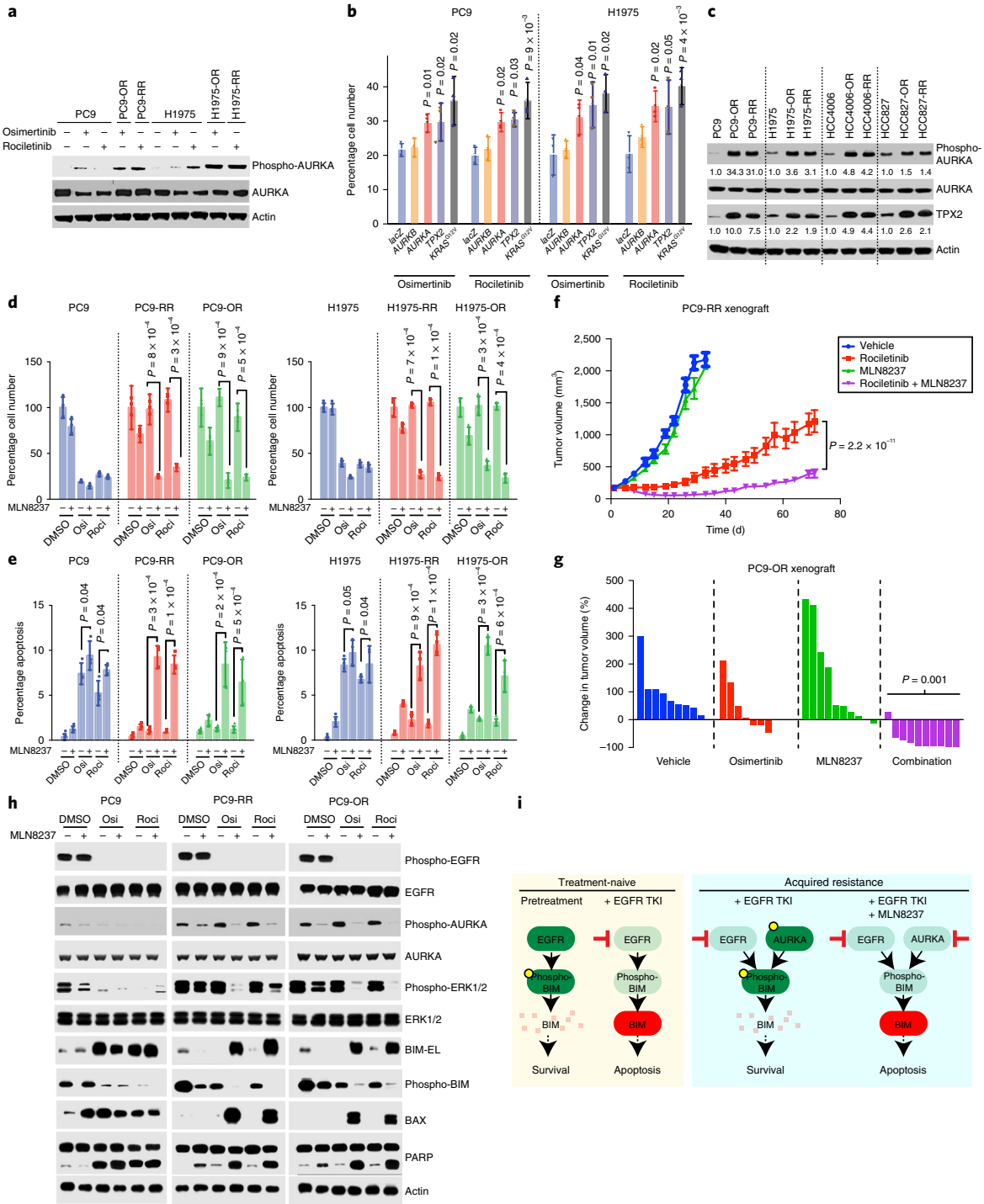

Fig. 2 | Activation of AURKA is sufficient to cause resistance to EGFR TKIs, and drug combinations induce apoptosis through BIM upregulation in vitro and in vivo. a, Immunoblot analysis of total AURKA and phospho-AURKA in PC9 and H1975 parental cell lines and those with acquired resistance that were treated with 1 μM of the indicated inhibitors for 24 h. **b**, Mean of cell proliferation of PC9 or H1975 cells transfected with plasmids expressing the indicated genes and treated with 1 μM EGFR TKIs for 72 h compared to DMSO-treated cells. The experiment was performed in $n = 3$ biologically independent samples. Significance is based on comparison to a *lacZ* control. **c**, Immunoblot analysis of four parental and eight cell lines with acquired resistance. Quantified intensities for phospho-AURKA and TPX2 relative to the parental cell line is shown. **d**, Proliferation of PC9 and H1975 parental, OR or RR cells treated with 1 μM osimertinib (osi) or rociletinib (roci), 30 nM of MLN8237 or the combination for 72 h compared to DMSO. Mean over $n = 3$ biologically independent samples. **e**, Apoptosis measured by YO-PRO-1 positivity in the same models and drug treatments as in **d** for 72 h. The mean from $n = 3$ biologically independent samples is shown. **f**, Mean tumor volume (mm^3) of PC9-RR xenografts during treatment with rociletinib (100 mg kg^{-1}), MLN8237 (10 mg kg^{-1}) or the combination. $n = 10$ tumors in the vehicle and rociletinib arms, and $n = 7$ in the MLN8237 and combination arms. **g**, Percentage change in tumor volume compared to baseline for individual PC9-OR cell xenografts treated for 11 d with osimertinib (5 mg kg^{-1}), MLN8237 (10 mg kg^{-1}) or the combination. The *P* value is based on comparing combination treatment to single-agent osimertinib treatment. **h**, Immunoblot of lysates from parental PC9, PC9-RR and PC9-OR cells treated with the indicated inhibitors or DMSO for 24 h. **i**, Proposed mechanism for the efficacy of the combination in cells with acquired resistance. *P* values are based on a two-tailed Student's *t*-test. The error bars represent the s.e.m. Blots are representative of at least two independent experiments. Full blots are shown in Supplementary Fig. 11.

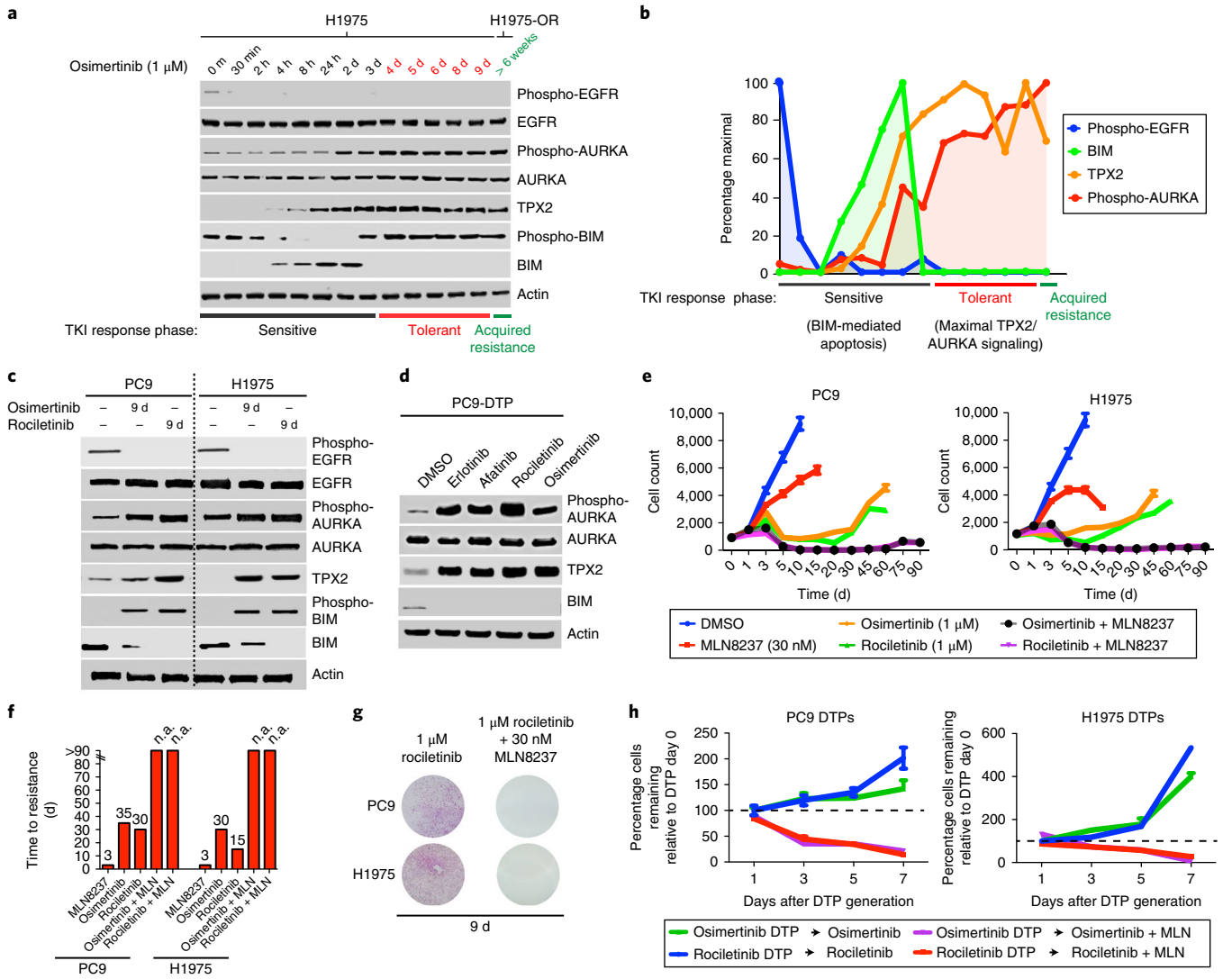

Fig. 3 | EGFR inhibition leads to the activation of TPX2 and AURKA during establishment of drug tolerance where it is necessary for survival and emergence of acquired resistance in vitro. a, Immunoblot of lysates from H1975 cells treated with osimertinib between 0 and 9 d and in H1975-OR cells, which have undergone continual treatment with osimertinib for >6 weeks. **b**, Quantification of the indicated molecules in **a** normalized to actin and scaled by maximal intensity. **c**, Immunoblot of indicated molecule lysates from drug-tolerant PC9 or H1975 cells that persist after treatment with 1 μM of the indicated agents for 9 d or in the parental cell line. **d**, Immunoblot of PC9 DTP cells formed by treatment with 1 μM of the EGFR inhibitors erlotinib (first-generation), afatinib (second-generation) and rociletinib or osimertinib (both third-generation) for 9 d. **e**, Growth of PC9 or H1975 cells in culture over time after plating and treatment with the indicated drugs. The mean over $n = 4$ biologically independent samples per time point is shown. **f**, Time to resistance defined as days to reach exponential growth in various treatment conditions. n.a., resistance not achieved after 90 d. **g**, Clonogenic growth of PC9 and H1975 cells treated with either 1 μM rociletinib or the combination of rociletinib and 30 nM MLN8237 for 9 d. Images represent $n = 2$ independent experiments. **h**, DTP PC9 or H1975 cells were generated through 9 d of treatment with 1 μM of osimertinib or rociletinib and then exposed to either 1 μM EGFR TKI alone or with the addition of 30 nM MLN8237 for up to 7 d. The mean of the percentage of cells remaining relative to day 0 calculated from $n = 4$ biologically independent samples per time point is shown. Error bars, s.e.m. Images in **c** and **d** are representative of at least two independent experiments. Full blots are shown in Supplementary Fig. 11.

in TPX2 followed by activation of AURKA peaking during the establishment of drug tolerance and maintained into acquired resistance (Fig. 3b). These data indicate that AURKA activation emerges after chronic EGFR inhibition and is maintained in drug-tolerant cells and those with acquired resistance.

Since high levels of TPX2 and AURKA cause mitotic errors and polyploidy[34,35], we hypothesized that its abnormal levels should also leave a signature of defects associated with mitotic stress. We surveyed for mitotic defects induced by EGFR TKI treatment and in cells with acquired resistance. EGFR TKI treatment for 72 h resulted in an accumulation of errors in centrosome biogenesis, spindle assembly and chromosome segregation in parental models and those with acquired resistance (Supplementary Fig. 7a,b and Supplementary Table 2), indicating that mitotic stress is a feature of EGFR inhibition. Upon EGFR inhibition, errors in mitosis led to the generation of polyploid cells (Supplementary Fig. 7c), which were phenocopied by overexpression of AURKA or TPX2 in parental cells, implying causation (Supplementary Fig. 7d,e). These data indicate that cells with acquired resistance emerge from drug-tolerant cells through the AURKA-dependent suppression of BIM, coincident with mitotic stress driven by abnormal levels of TPX2 and AURKA.

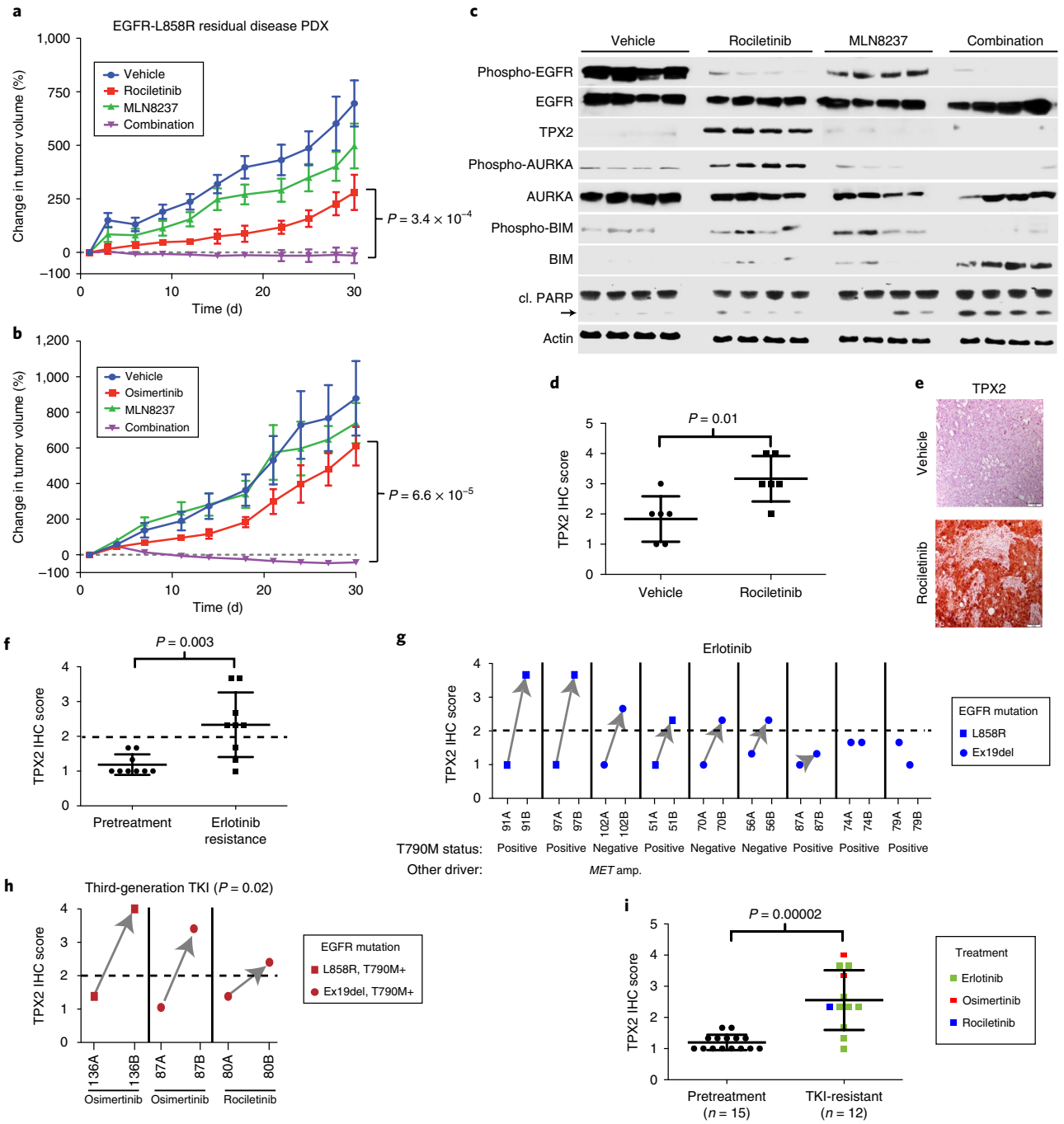

Fig. 4 | Clinical potential of combined EGFR and Aurora kinase inhibition on residual disease and acquired resistance. a, Growth of a PDX derived from a patient with an EGFR-L858R-mutant lung adenocarcinoma displaying an incomplete response to erlotinib biopsied at the point of residual disease. Mice were treated with 100 mg kg^{-1} rociletinib, 10 mg kg^{-1} MLN8237 or the combination of rociletinib and MLN8237 for 30 d. The *P* value is based on the comparison of combination to rociletinib alone. The averages over six tumors per arm are shown. **b**, Growth of individual PDX tumors treated with 1 mg kg^{-1} osimertinib, 10 mg kg^{-1} MLN8237 or the combination for 30 d. The *P* value is based on the comparison of combination to osimertinib alone. The averages over four tumors in the osimertinib arm and six tumors in all others are shown. **c**, Immunoblot of lysates from individual PDX tumors harvested 30 d after the initiation of treatment with the indicated compounds. cl. PARP, cleaved PARP. Images represent $n = 4$ independent tumors. Immunoblotting was performed once. **d**, Mean TPX2 levels from PDX tumors based on quantification of immunohistochemical staining. **e**, Representative image of TPX2 IHC from PDX tumors treated with the indicated agents. Images taken at ×20 magnification. Scale bar, 100 μM. Data are representative of six independent tumors. **f**, Mean TPX2 IHC scores from nine matched tumor samples from patients with EGFR-mutant lung adenocarcinoma taken at the time of diagnosis and at the time of relapse to erlotinib. **g**, TPX2 IHC scores of patient tumor tissue obtained before (ending with A) and on relapse when treated with erlotinib (ending with B). The same numbers indicate tumors from the same patient. Known genetic drivers of resistance based on genomic analysis are indicated. *MET* amp., *MET* amplification. **h**, Quantification of TPX2 IHC scores from human tumor samples taken from patients with EGFR-mutant lung adenocarcinoma patients at the time of diagnosis (ending with A) and at the time of relapse after treatment with either osimertinib or rociletinib (ending with B). **i**, Mean TPX2 IHC scores from all tumors taken from patients with EGFR-mutant lung adenocarcinoma before treatment and after resistance developed to the indicated TKIs. All data points are the mean, with the error bars representing the s.e.m. in **a** and **b** and the s.d. in **d**, **f** and **i**. *P* values are based on a two-tailed Student's *t*-test. Full blot images are shown in Supplementary Fig. 11.

Because AURKA became activated during drug tolerance, we hypothesized that AURKA might also be necessary for the formation and survival of drug-tolerant cells. While osimertinib and rociletinib drug-tolerant persister (DTP) cells[12] maintained EGFR inhibition and suppressed BIM-mediated apoptosis, they also displayed increased levels of phospho-AURKA and TPX2 (Fig. 3c). We observed this mechanism of tolerance to EGFR inhibition with other generations of EGFR inhibitors, including erlotinib and afatinib (Fig. 3d). To determine whether AURKA inhibition blocks the emergence of acquired resistance in EGFR TKI-naive NSCLC cells, we treated single-cell derived PC9 and H1975 cells with either single-agent EGFR TKI or MLN8237 or their combination over a period of 13 weeks and measured the rate of outgrowth of resistant clones. Combination treatment enhanced the magnitude of the response and delayed the emergence of resistance compared to monotherapy (Fig. 3e,f). This was because the combination increased the proportion of cells displaying evidence of apoptosis over the course of treatment, leading to a reduction in the formation of drug-tolerant, residual cells and was independent of which EGFR or Aurora kinase inhibitor was used (Fig. 3g and Supplementary Fig. 8a–c). Combination treatment was also effective in eradicating previously formed DTP cells with near complete elimination within 1 week, indicating that AURKA activity is necessary for their survival (Fig. 3h). These data suggest that the combination of EGFR TKI and Aurora kinase inhibitors administered simultaneously or in sequence at the time of residual disease may be an effective means to enhance the initial response and forestall acquired resistance.

We next explored the contribution of AURKA activation in clinical residual disease and progression. We tested an EGFR-L858R-positive and EGFR-T790M-negative patient-derived xenograft (PDX) tumor model from a residual mass obtained from a patient demonstrating an incomplete response to erlotinib[19]. Rociletinib treatment only modestly impaired tumor growth, indicating cross-resistance between erlotinib and rociletinib in this model. In contrast, the combination robustly decreased tumor growth compared to rociletinib alone ($P = 3.4 \times 10^{-4}$) and in most cases induced tumor regression with no observed toxicity on the basis of weight (Fig. 4a and Supplementary Fig. 9a,b). Combination treatment induced apoptosis as evidenced by increased staining for cleaved caspase-3 as well as loss of Ki-67 staining in tumor tissue (Supplementary Fig. 9c,d). We also observed efficacy and lack of toxicity using osimertinib in combination with MLN8237 ($P = 6.6 \times 10^{-5}$) (Fig. 4b and Supplementary Fig. 9e,f).

Consistent with the adaptive resistance observed in vitro, tumors treated with rociletinib for 30 d had lower phospho-EGFR levels and an increase in phospho-AURKA and TPX2 levels compared to vehicle alone (Fig. 4c). Enhanced TPX2 levels in rociletinib-treated tumors were also evident through immunohistochemistry (IHC) (Fig. 4d,e). EGFR suppression also induced mitotic stress in vivo, and there was a significant increase in the number of abnormal mitoses quantified via H&E staining (Supplementary Fig. 9g,h). The combination also induced apoptosis as evidenced by suppression of phospho-BIM, increased total BIM and cleaved PARP compared to either single agent (Fig. 4c). These results establish mechanistic equivalence between processes occurring in vitro with those occurring in patient residual disease and indicate that pharmacologically targeting AURKA at the point of maximal response or residual disease may be a viable clinical strategy to deepen responses.

We next sought to establish the clinical relevance of heightened TPX2/AURKA signaling in mediating acquired resistance to EGFR inhibition in NSCLC. Staining and automated quantification of TPX2 levels in matched diagnosis and relapse samples from nine patients with advanced-stage EGFR-mutant NSCLC who underwent treatment with erlotinib revealed a significant increase in TPX2 levels after acquired resistance compared to pretreatment ($P = 0.003$) (Fig. 4f). Using a threshold TPX2 score of 2, which was higher than what we observed in all nine pretreatment samples, we observed TPX2 positivity in six out of nine cases (Fig. 4g and Supplementary Fig. 10a). Interestingly, we observed increased TPX2 levels in three cases that also displayed EGFR-T790M-positivity or *MET* amplification upon relapse, suggesting that nongenetic AURKA activation as a driver may co-occur with other genetic drivers of acquired resistance. In three acquired resistance cases to third-generation inhibitors (two osimertinib and one rociletinib), all three were TPX2-positive and were increased compared to pretreatment ($P = 0.02$) (Fig. 4h and Supplementary Fig. 10b). Together, resistance was associated with an increase in TPX2 regardless of the EGFR TKI used (positivity in 75% of cases, $P = 0.00002$) (Fig. 4i). These data suggest that AURKA activation via TPX2 is a feature of most acquired resistant EGFR-mutant lung cancers regardless of therapy. We propose that TPX2 could be used as a biomarker to select patients for combination therapy with an EGFR TKI and an Aurora kinase inhibitor in EGFR-mutant lung adenocarcinoma.

In summary, our findings have important implications for intercepting EGFR TKI resistance in patients with NSCLC, offering an alternative approach to combat the emergence of resistance. In light of observations that multiple distinct mechanisms of drug resistance can co-occur within the same patient at the time of relapse[5–8], AURKA activation might co-occur with other factors driving resistance or could even provide a mechanism on which such resistance-causing mutations could appear, giving rise to multiple genetically distinct clones[11]. The maintenance of residual disease by AURKA may provide a fertile ground for the formation of such resistance-causing mutations, potentially through a late-emerging resistance model[10,11]. For example, mitotic abnormalities catalyzed by AURKA hyperactivity may give rise to gene amplifications that have been observed in patients progressing on EGFR inhibitors. Since mitotic errors lead to chromosomal instability contributing to disease progression and drug resistance[36], resistance driven by AURKA may contribute to tumor heterogeneity and promote the generation of distinct clones harboring different genetic drivers of drug resistance. If correct, this adaptive response to EGFR inhibition could actually enhance tumor heterogeneity. Data from our study and others demonstrate that AURKA contributes to a number of pathways and processes previously associated with resistance to EGFR inhibition, including NF-κB, ERK and EMT[26,37]. Therefore, it appears that AURKA is associated with a number of seemingly disparate mechanisms of acquired resistance, warranting further investigation.

Our results call for clinical trials testing the combination of Aurora kinase and EGFR inhibitors in EGFR-mutant lung adenocarcinoma, up front, at the point of residual disease and after acquired resistance in tumors harboring high levels of TPX2. Patients progressing on first- and third-generation EGFR TKIs often have high levels of TPX2, indicating therapeutic relevance in a significant fraction of acquired resistant, immunotherapy-refractory[38] lung cancers. As single-agent therapies, Aurora kinase inhibitors have reached phase 3 clinical trials[39,40] and have nonoverlapping toxicity profiles with EGFR inhibitors. We propose that the most effective use of this combination should be directed toward eliminating residual cancer cells before they acquire genetic mechanisms of resistance that could be polyclonal and heterogeneous in nature. While clinical studies are necessary to determine the degree to which this combination strategy can delay the onset of resistance in patients, these results call to action a proactive paradigm aimed at preventing resistance rather than the current reactive paradigm of intercepting and treating drug resistance incrementally.

Online content

Any methods, additional references, Nature Research reporting summaries, source data, statements of data availability and associated accession codes are available at https://doi.org/10.1038/s41591-018-0264-7.

Received: 13 September 2017; Accepted: 4 October 2018;
Published online: 26 November 2018

References

1. Jänne, P. A. et al. AZD9291 in EGFR inhibitor-resistant non-small-cell lung cancer. *N. Engl. J. Med.* **372**, 1689–1699 (2015).
2. Sequist, L. V. et al. Rociletinib in EGFR-mutated non-small-cell lung cancer. *N. Engl. J. Med.* **372**, 1700–1709 (2015).
3. Rosell, R. et al. Erlotinib versus standard chemotherapy as first-line treatment for European patients with advanced EGFR mutation-positive non-small-cell lung cancer (EURTAC): a multicentre, open-label, randomised phase 3 trial. *Lancet Oncol.* **13**, 239–246 (2012).
4. Sequist, L. V. et al. Genotypic and histological evolution of lung cancers acquiring resistance to EGFR inhibitors. *Sci. Transl. Med.* **3,** 75ra26 (2011).
5. Blakely, C. M. et al. Evolution and clinical impact of co-occurring genetic alterations in advanced-stage EGFR-mutant lung cancers. *Nat. Genet.* **49**, 1693–1704 (2017).
6. Burrell, R. A. & Swanton, C. Tumour heterogeneity and the evolution of polyclonal drug resistance. *Mol. Oncol.* **8**, 1095–1111 (2014).
7. Chabon, J. J. et al. Circulating tumour DNA profiling reveals heterogeneity of EGFR inhibitor resistance mechanisms in lung cancer patients. *Nat. Commun.* **7**, 11815 (2016).
8. Yang, Z. et al. Investigating novel resistance mechanisms to third-generation EGFR tyrosine kinase inhibitor osimertinib in non-small cell lung cancer patients. *Clin. Cancer Res.* **24**, 3097–3107 (2018).
9. Bivona, T. G. & Doebele, R. C. A framework for understanding and targeting residual disease in oncogene-driven solid cancers. *Nat. Med.* **22**, 472–478 (2016).
10. Hata, A. N. et al. Tumor cells can follow distinct evolutionary paths to become resistant to epidermal growth factor receptor inhibition. *Nat. Med.* **22**, 262–269 (2016).
11. Ramirez, M. et al. Diverse drug-resistance mechanisms can emerge from drug-tolerant cancer persister cells. *Nat. Commun.* **7**, 10690 (2016).
12. Sharma, S. V. et al. A chromatin-mediated reversible drug-tolerant state in cancer cell subpopulations. *Cell* **141**, 69–80 (2010).
13. Kim, T. M. et al. Mechanisms of acquired resistance to AZD9291: a mutation-selective, irreversible EGFR inhibitor. *J. Thorac. Oncol.* **10**, 1736–1744 (2015).
14. Li, L. et al. Transformation to small-cell carcinoma as an acquired resistance mechanism to AZD9291: a case report. *Oncotarget* **8**, 18609–18614 (2017).
15. Piotrowska, Z. et al. Heterogeneity underlies the emergence of EGFR T790 wild-type clones following treatment of T790M-positive cancers with a third-generation EGFR inhibitor. *Cancer Discov.* **5**, 713–722 (2015).
16. Thress, K. S. et al. Acquired EGFR C797S mutation mediates resistance to AZD9291 in non-small cell lung cancer harboring EGFR T790M. *Nat. Med.* **21**, 560–562 (2015).
17. Niederst, M. J. & Engelman, J. A. Bypass mechanisms of resistance to receptor tyrosine kinase inhibition in lung cancer. *Sci. Signal.* **6**, re6 (2013).
18. Bivona, T. G. et al. FAS and NF-κB signalling modulate dependence of lung cancers on mutant EGFR. *Nature* **471**, 523–526 (2011).
19. Blakely, C. M. et al. NF-κB-activating complex engaged in response to EGFR oncogene inhibition drives tumor cell survival and residual disease in lung cancer. *Cell Rep.* **11**, 98–110 (2015).
20. Shien, K. et al. Acquired resistance to EGFR inhibitors is associated with a manifestation of stem cell-like properties in cancer cells. *Cancer Res.* **73**, 3051–3061 (2013).
21. Chen, J. et al. AURKA upregulation plays a role in fibroblast-reduced gefitinib sensitivity in the NSCLC cell line HCC827. *Oncol. Rep.* **33**, 1860–1866 (2015).
22. Eberlein, C. A. et al. Acquired resistance to the mutant-selective EGFR inhibitor AZD9291 is associated with increased dependence on RAS signaling in preclinical models. *Cancer Res.* **75**, 2489–2500 (2015).
23. Karaman, M. W. et al. A quantitative analysis of kinase inhibitor selectivity. *Nat. Biotechnol.* **26**, 127–132 (2008).
24. Fu, J., Bian, M., Jiang, Q. & Zhang, C. Roles of Aurora kinases in mitosis and tumorigenesis. *Mol. Cancer Res.* **5**, 1–10 (2007).
25. Sharifnia, T. et al. Genetic modifiers of EGFR dependence in non-small cell lung cancer. *Proc. Natl. Acad. Sci. USA* **111**, 18661–18666 (2014).
26. Nikonova, A. S., Astsaturov I.Serebriiskii, I. G., Dunbrack, R. L.Jr. & Golemis, E. A. Aurora A kinase (AURKA) in normal and pathological cell division. *Cell. Mol. Life Sci.* **70**, 661–687 (2013).
27. Stewart, S. & Fang, G. Anaphase-promoting complex/cyclosome controls the stability of TPX2 during mitotic exit. *Mol. Cell. Biol.* **25**, 10516–10527 (2005).
28. Zhou, Y., Ching, Y. P., Chun, A. C. & Jin, D. Y. Nuclear localization of the cell cycle regulator CDH1 and its regulation by phosphorylation. *J. Biol. Chem.* **278**, 12530–12536 (2003).
29. Ercan, D. et al. Reactivation of ERK signaling causes resistance to EGFR kinase inhibitors. *Cancer Discov.* **2**, 934–947 (2012).
30. Costa, D. B. et al. BIM mediates EGFR tyrosine kinase inhibitor-induced apoptosis in lung cancers with oncogenic EGFR mutations. *PLoS Med.* **4**, 1669–1679 (2007).
31. Cragg, M. S., Kuroda, J., Puthalakath, H., Huang, D. C. & Strasser, A. Gefitinib-induced killing of NSCLC cell lines expressing mutant EGFR requires BIM and can be enhanced by BH3 mimetics. *PLoS Med.* **4**, 1681–1689 (2007).
32. Hübner, A., Barrett, T., Flavell, R. A. & Davis, R. J. Multisite phosphorylation regulates Bim stability and apoptotic activity. *Mol. Cell* **30**, 415–425 (2008).
33. Moustafa-Kamal, M., Gamache, I., Lu, Y., Li, S. & Teodoro, J. G. BimEL is phosphorylated at mitosis by Aurora A and targeted for degradation by βTrCP1. *Cell Death Differ.* **20**, 1393–1403 (2013).
34. Anand, S., Penrhyn-Lowe, S. & Venkitaraman, A. R. AURORA-A amplification overrides the mitotic spindle assembly checkpoint, inducing resistance to Taxol. *Cancer Cell.* **3**, 51–62 (2003).
35. Gruss, O. J. et al. Chromosome-induced microtubule assembly mediated by TPX2 is required for spindle formation in HeLa cells. *Nat. Cell Biol.* **4**, 871–879 (2002).
36. Lee, A. J. et al. Chromosomal instability confers intrinsic multidrug resistance. *Cancer Res.* **71**, 1858–1870 (2011).
37. D'Assoro, A. B. et al. The mitotic kinase Aurora-A promotes distant metastases by inducing epithelial-to-mesenchymal transition in ERα$^+$ breast cancer cells. *Oncogene* **33**, 599–610 (2014).
38. Lee, C. K. et al. Clinical and molecular characteristics associated with survival among patients treated with checkpoint inhibitors for advanced non-small cell lung carcinoma: a systematic review and meta-analysis. *JAMA Oncol.* **4**, 210–216 (2018).
39. Bavetsias, V. & Linardopoulos, S. Aurora kinase inhibitors: currents status and outlook. *Front. Oncol.* **5**, 278 (2015).
40. Melichar, B. et al. Safety and activity of alisertib, an investigational aurora kinase A inhibitor, in patients with breast cancer, small-cell lung cancer, non-small-cell lung cancer, head and neck squamous-cell carcinoma, and gastro-oesophageal adenocarcinoma: a five-arm phase 2 study. *Lancet Oncol.* **16**, 395–405 (2015).

Acknowledgements

We thank members of the Bandyopadhyay laboratory for helpful discussions and technical assistance. We also thank J. Gordon from the LCA microscopy core for technical assistance and reagents. This work was supported by National Cancer Institute grant nos. U01CA168370 (S.B.), NIGMS R01GM107671 (S.B.), R01CA169338 (T.G.B) and U54CA224081 (S.B., T.G.B).

Author contributions

Project conception: K.N.S. and S.B. Performance of experiments: K.N.S., R.B., J.W., J. Rotow, J. Rohrberg, V.E.W., H.J.D., J.G., V.O., G.H., M.M.M., A.M., J.K., H.J.H., L.R. and G.K. Data analysis and interpretation: K.N.S., H.J.D., S.K., A.K., S.D. and G.K. Manuscript writing: K.N.S. and S.B. Manuscript finalization: all authors. Study supervision: T.C.H., A.D.S., F.M., A.G., C.M.B., T.G.B and S.B. Funding: S.B.

Competing interests

H.J.H., L.R., A.D.S. and T.C.H. are employees of Clovis Oncology. S.B. recieves funding and/or has a consultancy relationship with Ideaya Biosciences and Pfizer.

Additional information

Supplementary information is available for this paper at https://doi.org/10.1038/s41591-018-0264-7.

Reprints and permissions information is available at www.nature.com/reprints.

Correspondence and requests for materials should be addressed to S.B.

Publisher's note: Springer Nature remains neutral with regard to jurisdictional claims in published maps and institutional affiliations.

Methods

Cell culture and compounds. H1975, HCC827 and HCC4006 cells were obtained from ATCC. PC9 cells were a gift from F. Koizumi (National Cancer Center Research Institute and Shien-Lab, Tokyo, Japan). PC9 parental cell line identity was confirmed by short tandem repeat analysis (Genetica). Cells were used for no longer than 12 months before being replaced and were routinely tested for *Mycoplasma* to ensure the accuracy of experimental data. Rociletinib was obtained from Clovis Oncology. Erlotinib, afatinib and osimertinib (AZD9291) were purchased from Selleck Chemicals.

Generation of cells with acquired resistance and drug-tolerant cells. Cells with acquired resistance were derived by treating individual cell lines with increasing concentrations of rociletinib or osimertinib starting at 50 nM, followed by a stepwise dose escalation every 48 h up to 1 μM. Cell lines with acquired resistance that were derived from rociletinib treatment (PC9-RR, H1975-RR, HCC4006-RR, HCC827-RR) or osimertinib treatment (PC9-OR, H1975-OR, HCC4006-OR, HCC827-OR) were maintained in 1 μM of the respective drug. To generate DTP cells, parental PC9 and H1975 were treated with 1 μM of erlotinib, afatinib, rociletinib and osimertinib for 9 d, according to protocols described previously[12]. Cells were washed and replenished with fresh drug every 48 h.

Cell proliferation and apoptosis assays. Cell lines were seeded in 384-well assay microplates at a density of 1,000 cells per well in a total volume of 40 μl per well and incubated at 37 °C, 5% CO_2 overnight. Following drug exposure, proliferation was measured by staining with Hoechst 33342 (Thermo Fisher Scientific) nuclear dye; apoptosis was measured using YO-PRO-1 early apoptosis dye (Thermo Fisher Scientific) and analyzed using a CellInsight High-Content Microscope (Thermo Fisher Scientific) for the indicated time. IC_{50} values were determined using Prism version 6.0 (GraphPad). For drug synergy, fixed-dose ratios were used to determine five different drug combinations. Following 72 h of drug exposure, proliferation and cell death were measured by staining with Hoechst 33342 nuclear dye and YO-PRO-1, respectively, and analyzed using a CellInsight High-Content Microscope. Synergistic, additive or antagonistic effects were determined using the combination index method devised by Chou and Talalay[41].

Combination drug screen. H1975-RR cells were seeded in 384-well microplates at a density of 1,000 cells per well in the presence of 2 μM rociletinib or vehicle; after 24 h, they were exposed to three different doses of compounds from a 90-drug library for 72 h. At the end of this period, nuclei were stained with Hoechst 33342 and counted using a CellInsight High-Content Microscope. The screen was repeated three times using varying library concentrations of 5 μg ml^{-1}, 500 ng ml^{-1} and 50 ng ml^{-1}, and each combination was measured in quadruplicate. Raw cell numbers were median-normalized on a per-plate basis. For each compound in the library, the relative cell number in the DMSO plate was compared with the number in the rociletinib plate using a two-tailed Student's *t*-test. A synergy score was developed based on the $-\log_{10}$ of the *P* value of this *t*-test and was signed to indicate synergistic inhibition of growth (positive score) or antagonism (negative score). The reported synergy score is based on the average of scores over three different library concentrations.

Clonogenic growth assay. Colony outgrowth assays were performed using crystal violet staining and quantification. Briefly, cells were seeded in 12-well microplates at a density of 1,000 cells per well. Appropriate drugs were added after an additional 24 h. Cells were exposed to drug or DMSO for 9–10 d, with medium change and fresh drug added every 3 d. Cells were fixed with 4% formaldehyde and stained with 0.5% crystal violet. Pictures of stained cells were taken using an EPSON Perfection V600 scanner. Growth was quantified by dissolving crystal violet in 0.1% SDS and absorbance was quantified at 590 nm using a spectrophotometer and normalized to DMSO treatment.

Immunoblot. Cells for immunoblots were collected and lysed in lysis buffer containing 1 mol l^{-1} Tris-HCl buffer, pH 7.6, 0.5 mol l^{-1} EDTA, 5 mol l^{-1} NaCl, 1% NP-40 and 1% Triton X-100, supplemented with protease and phosphatase inhibitors (Calbiochem). Samples were sonicated and then centrifuged at 14,000 r.p.m. for 10 min at 4 °C. Protein concentrations were determined by Bradford assay (Bio-Rad). Equal amounts of protein (10–40 μg) were loaded onto SDS–polyacrylamide gel electrophoresis gels, transferred to a polyvinylidene difluoride membrane (Bio-Rad) and incubated with the indicated primary antibodies. Proteins were detected via incubation with horseradish peroxidase–conjugated secondary antibodies, Clarity Western ECL Blotting Substrates (Bio-Rad) or SuperSignal West Femto Maximum Sensitivity Chemiluminescent Substrate (Thermo Fisher Scientific). Antibodies for phospho-EGFR (Y1068), phospho-ERK1/2 (T202/Y204), ERK1/2, phospho-Akt (S473), Akt, cleaved PARP, phospho-AURKA (T288), AURKA, phospho-Rb (S780), BIM, phospho-BIM (S69), BAX, vimentin, phospho-NF-κB p65 (S536), NF-κB p65, pan phospho-AURKA/B/C (T288/T232/T198), CD44 and histone H3 (9715) were purchased from Cell Signaling Technology; TPX2 and pan total AURKA/B/C were purchased from Sigma-Aldrich; EGFR, NEDD9/Cas-L, AJUBA, PAK-1, CD24, CD133, β-tubulin and p53 were purchased from Santa Cruz Biotechnology; FZR1/CDH1 was purchased from Abcam; and V5 tag was purchased from Thermo Fisher Scientific. Band intensities were quantified using Adobe Photoshop CS3. Phospho-receptor tyrosine kinase arrays were performed according to the manufacturer's protocol (R&D Systems).

Cell cycle synchronization and analysis. For double thymidine block, cells were seeded and 2 mM thymidine was added; later, thymidine was released from this block by washing the cells three times with PBS and adding complete media followed by a second thymidine block and release. For synchronization using serum starvation and release, cells were kept in serum-free media for 48 h. To synchronize cells in the G1/S phase, cells were released for 2 h; to synchronize cells in the G2/M phase, cells were released for 8 h followed by drug treatment. In all cases, the expected cell cycle was validated using fluorescence-activated cell sorting. For cell cycle analysis, cells were fixed in cold ethanol and resuspended in propidium iodide/RNase staining solution (Cell Signaling Technology). After incubation for 15 min at room temperature in the dark, flow cytometric analysis was performed on a FACS Aria II Flow Cytometer (BD Biosciences). Flow cytometry data were analyzed with the FlowJo software to measure polyploidy (>4 N).

Plasmid transfections. LacZ, TPX2, AURKA, AURKB, AJUBA, NEDD9, PAK-1 and KRAS-G12V were obtained in a pLX304 backbone from Addgene; 1 μg per well of plasmids were transfected with 0.1% FuGENE HD transfection reagent (Promega) for 48 h before further analysis.

Quantification of mitotic defects. Cells were plated overnight on a tissue culture–treated 8-well chamber slide (Thermo Fisher Scientific). After 72 h of drug treatment, cells were washed with PBS and fixed by with ice-cold methanol at −20 °C for 3 min. Following fixation, cells were permeabilized with PBS and 0.1% Triton X-100 for 3 min, blocked in PBS with Tween 20 (PBS, 5% BSA, 0.1% Triton X-100) for 30 min and then incubated with primary antibodies in blocking buffer for 90 min. Cells were washed with PBS and incubated with species-specific fluorescent secondary antibodies (Alexa-conjugated; Thermo Fisher Scientific). DNA was stained with Hoechst 33342 (1:5,000) for 5 min in PBS. Coverslips were mounted with ProLong Antifade mountant (Thermo Fisher Scientific). Antibodies were anti-α-tubulin (1:500; Sigma-Aldrich) and anti-γ-tubulin (1:500; Sigma-Aldrich). Images were collected with a ZEISS Cell Observer using the 404, 488 and 561 nm laser.

Human tissue and IHC. All patient tumor samples analyzed were obtained under institutional review board–approved protocols with informed consent obtained from each patient under the guidance of the University of California, San Francisco (UCSF). All relevant ethical regulations were followed. The mutational status of EGFR or other known drivers or resistance was determined using either FoundationOne (Foundation Medicine) or UCSF pathology. Tissues were fixed in 10% formalin overnight and embedded in paraffin. Tissue sections of PDX and patient samples were sectioned on slides with 4-μm thickness. The paraffin sections were deparaffinized in xylene and rehydrated in a graded alcohol series, boiled with 10 mmol l^{-1} of citrate buffer (pH 6) for 10 min and treated with 0.3% H_2O_2 for 10 min. The steps were performed using the Envision two-step method using the Envision and DAB Color kit (Gene Tech). The TPX2 antibody (1:200 dilution; Sigma-Aldrich), cleaved caspase-3 (1:200 dilution; Cell Signaling Technology) and mouse monoclonal antibody Ki67 (1:100 dilution; Leica Biosystems) were used; PBS was used as the negative control. Images were captured using a ZEISS Axio Imager M1, and immunoreactivity was evaluated with IHC Profiler[42] as an Image J plug-in in a blinded manner. The evaluation was based on staining intensity and the extent of staining. The staining area was scored using the following scale: 0, 0–10% of tissue stained positive; 1, 10–20% stained positive; 2, 20–40% stained positive; 3, 40–70% stained positive; and 4, >70% positive cells. The sum of staining score index (intensity + extent) was designated as follows: 0–2, negative expression; 3–4, strong expression. The IHC score was generated from three different areas of the slides and the average score was calculated for each sample.

Mouse xenograft studies. Cell line xenograft experiments were performed in female C.B-17 SCID mice aged 8 weeks by injecting 5×10^6 PC9-RR, PC9-OR tumor cells within 50% Matrigel gelatinous protein mixture (Corning). Tumors were allowed to grow until they reached a minimum volume of 150 mm^3, and mice were randomized to receive treatment by oral gavage 7 d per week for 71 days. Rociletinib was formulated using 5% DMSO, 15% Solutol HS 15 (Sigma-Aldrich) in 80% water; osimertinib was formulated in 1% DMSO, 30% polyethylene glycol 300 and 69% water. MLN8237 was formulated using 10% (2-hydroxypropyl)-β-cyclodextrin in water. Tumor growth was assessed twice weekly by caliper measurements. A minimum of ten tumors per treatment group were assessed for the duration of the study. For PDX, patient-derived tumor cells were engrafted subcutaneously into the flank of C.B-17 SCID mice. Tumors were allowed to grow until they reached a minimum volume of 200 mm^3; then, animals were randomly placed into control or treatment groups. Animals were treated daily for 30 d via oral gavage, and tumor volume was calculated daily using caliper measurements.

The percentage change in tumor growth was based on volumes calculated from the size on day 1 at the beginning of treatment. All animal studies were conducted in accordance with the UCSF Institutional Animal Care and Use Committee, and all relevant ethical regulations were followed.

Real-time PCR. RNA was isolated according to the manufacturer's instructions (TRIzol; Thermo Fisher Scientific); 1 µg of total RNA from each sample was subjected to first-strand complementary DNA synthesis according to the manufacturer's recommendations (Promega). Quantitative PCR was performed on a CFX96 Real-Time PCR Detection System (Bio-Rad) with a PrimeTime Gene Expression Master Mix (Integrated DNA Technologies) according to the manufacturer's protocol. TPX2 was amplified with the following primers: 5′-AGGGGCCCTTTGAACTCTTA-3′ (forward primer) and 5′-TGCTCTAAACAAGCCCCATT-3′ (reverse primer). 60S ribosomal protein L13a (L13aRPL13A) was used as an endogenous control with the following primers: 5′-CGGATTTGGTCGTATTGG-3′ (forward primer) and 5′-TCCTGGAAGATGGTGATG-3′ (reverse primer). AURKA was amplified with AGTTGGCAAACGCTCTGTCT (forward primer) and GTGCCACACATTGTGGTTCT (reverse primer). AURKB was amplified with TCCCTGTTCGCATTCAACCT (forward primer) and GTCCCACTGCTATTCTCCATCAC (reverse primer). AURKC was amplified with ACAACACCGGAACATCCTTC (forward primer) and TGCTGGTCCAACTTCTGATG (reverse primer). The cycling conditions were as follows: one cycle at 95 °C for 3 min; 40 cycles at 95 °C for 15 s and 60 °C for 60 s. The specificity of the PCR amplification was validated by the presence of a single peak in the melting curve analyses. Each real-time quantitative PCR experiment was repeated three times.

In vitro resistance assay. Single-cell-expanded PC9 and H1975 cells were plated in 96-well microplates at a density of 500 cells per well (~10% confluency), and drug treatment began the following day. Each treatment group had 12 replicates, and drug was replaced every 72–96 h. Each microplate was harvested at the end of day 1, 3, 5, 10, 15, 20, 30, 45, 60, 75 and 90 and cell proliferation was measured.

Reversibility of resistance. To test the reversibility of resistance, we seeded single-cell derived clones using a limited dilution method into 384-well microplates. Single-cell derived clones were allowed to expand in the absence or presence of drugs for 14 d. Once these single cells achieved about 80% confluence at the end of 14 d, a subset that had expanded in the absence of drug were tested for sensitization by adding 1 µM of respective EGFR TKI for 72 h. For each cell line, 96 single-cell clones were analyzed in each treatment condition.

Ras-guanosine triphosphate pull-down assay. Cells were washed twice in ice-cold PBS and lysed in 1% TX100-TNM lysis buffer (20 mmol/l^{-1} Tris, pH 7.5, 5 mmol l^{-1} $MgCl_2$, 150 mmol l^{-1} NaCl, 1% Triton X-100) supplemented with 1 mmol l^{-1} dithiothreitol and protease and phosphatase inhibitors (Sigma-Aldrich). Equal amounts of protein from each sample were added to 10 µl of packed GST-coupled Ras binding domain of Raf (GST-Raf-RBD) or Ral GDS-Rap binding domain (Ral-GDS-RBD) beads in 300–500 µl of 1% TX100-TNM lysis buffer and rotated at 4 °C for 1–2 h. Beads were washed three times with 1 ml cold lysis buffer and boiled in lithium dodecyl sulfate sample buffer (Thermo Fisher Scientific).

Subcellular fractionation. Nuclear and cytoplasmic fractions were prepared using the NE-PER Nuclear and Cytoplasmic Extraction Reagents (Thermo Fisher Scientific) according to the manufacturer's instructions. Protein concentration was quantitated using the Pierce BCA Protein Assay Kit (Thermo Fisher Scientific). Equal amounts of protein were loaded into each lane and separated on a 4–12% Bis-Tris gel (Thermo Fisher Scientific), then transferred onto a nitrocellulose membrane.

Reporting summary. Further information on research design is available in the Nature Research Reporting Summary linked to this article.

Data availability

All data generated or analyzed during this study are included in this published article and its supplementary information files. Cell lines generated in this study are available upon reasonable request from the authors.

References

41. Chou, T. C. Drug combination studies and their synergy quantification using the Chou–Talalay method. *Cancer Res.* **70**, 440–446 (2010).
42. Varghese, F., Bukhari, A. B., Malhotra, R. & De, A. IHC Profiler: an open source plugin for the quantitative evaluation and automated scoring of immunohistochemistry images of human tissue samples. *PLoS ONE* **9**, e96801 (2014).

nature research

Corresponding Author: Bandyopadhyay, Sourav

Date: Oct 2, 2018

Life Sciences Reporting Summary

Nature Research wishes to improve the reproducibility of the work we publish. This form is published with all life science papers and is intended to promote consistency and transparency in reporting. All life sciences submissions use this form; while some list items might not apply to an individual manuscript, all fields must be completed for clarity.

For further information on the points included in this form, see Reporting Life Sciences Research. For further information on Nature Research policies, including our data availability policy, see Authors & Referees and the Editorial Policy Checklist.

Experimental design

1. Sample size

   Describe how sample size was determined.

   For in vivo experiments each arm was designed to contain at least 6 tumors which we estimated to provide 90% power to detect a 20% difference in growth rate at p-value < 0.05.

2. Data exclusions

   Describe any data exclusions.

   We performed exome sequencing of the acquired resistant cell lines and did not ind any significant recurrent mutation. Hence we are not showing the data, but we mention this in our manuscript.

3. Replication

   Describe whether the experimental findings were reliably reproduced.

   Biological replications are as indicated in figure legends. All attempts at replication were successful.

4. Randomization

   Describe how samples/organisms/participants were allocated into experimental groups.

   Animals were randomized at the start of treatment. In figure 4b some animals in the combination arm had significantly larger tumors at the start of treatment. This bias does not impact the interpretation of the experiment.

5. Blinding

   Describe whether the investigators were blinded to group allocation during data collection and/or analysis.

   Mitotic errors and IHC scoring were performed in a blinded manner to avoid observation bias.

Note: all studies involving animals and/or human research participants must disclose whether blinding and randomization were used.

6. Statistical parameters

   For all figures and tables that use statistical methods, confirm that the following items are present in relevant figure legends (or the Methods section if additional space is needed).

n/a	Confirmed	
☐	☒	The exact sample size (*n*) for each experimental group/condition, given as a discrete number and unit of measurement (animals, litters, cultures, etc.)
☐	☒	A description of how samples were collected, noting whether measurements were taken from distinct samples or whether the same sample was measured repeatedly.
☐	☒	A statement indicating how many times each experiment was replicated
☐	☒	The statistical test(s) used and whether they are one- or two-sided (note: only common tests should be described solely by name; more complex techniques should be described in the Methods section)
☐	☒	A description of any assumptions or corrections, such as an adjustment for multiple comparisons
☐	☒	The test results (e.g. *p* values) given as exact values whenever possible and with confidence intervals noted
☐	☒	A summary of the descriptive statistics, including central tendency (e.g. median, mean) and variation (e.g. standard deviation, interquartile range)
☐	☒	Clearly defined error bars

See the web collection on statistics for biologists for further resources and guidance.

Software

Policy information about availability of computer code

7. Software

Describe the software used to analyze the data in this study.	Statistical analyses for this study were performed using GraphPad Prism 6 (version 6.0g). IHC profiler plug-in Fiji Image J (version 2.0.0-rc-43/1.51p). FlowJo was version 10.2.

For all studies, we encourage code deposition in a community repository (e.g. GitHub). Authors must make computer code available to editors and reviewers upon request. The *Nature Methods* guidance for providing algorithms and software for publication may be useful for any submission.

Materials and reagents

Policy information about availability of materials

8. Materials availability

Indicate whether there are restrictions on availability of unique materials or if these materials are only available for distribution by a for-profit company.	All material are available from standard available sources and cell lines available upon reasonable request.

9. Antibodies

Describe the antibodies used and how they were validated for use in the system under study (i.e. assay and species).	Antibodies for pEGFR (Y1068; 3777, D7A5, 1:500), pERK1/2 (T202/Y204; 4370, D13.14.4E, 1:1000), ERK1/2 (9102, 1:1000), pAKT (S473; 4060, D9E, 1:1000), AKT (9272, 1:1000), PARP (5625, D64E10, 1:1000), pAURKA (T288; 3079, C39D5, 1:250), AURKA (4718, 1G4, 1:500), pan-pphospho AURKA/B/C (T288/T232/T198, 2914, D13A11, 1:500) pRb (S780; 9307, 1:1000), BIM (2933, C34C5, 1:500), pBIM (S69; 4585, D7E11, 1:300), BAX (5023, D2E11, 1:1000), Vimentin (5741, D21H3, 1:1000), p-p65 (S536; 3033, 93H1, 1:500), p65 (8242, D14E12, 1:1000), CD44 (3570, 156-3C11, 1:1000), Histone H3 (9715, 1:1000) were purchased from Cell Signaling Technology; TPX2 (HPA005487, 1:250) and pan total AURKA/B/C (HPA002636, 1:1000) were purchased from Sigma; EGFR (SC-03, 1:1000), NEDD9 (sc-33657, 14A11, 1:200), AJUBA (sc-398008, B-3, 1:100), PAK1 (sc-166174, D-8, 1:500), CD24 (sc-19585, SN3, 1:300), CD133 (sc-30219, M-286, 1:1000), B-tubulin (sc-9104, H-235, 1:500), p53 (sc-126, DO-1, 1:500) were purchased from Santa Cruz biotechnology and FZR1/CDH1 (ab3242, 1:50) from Abcam and V5 tag (46-0705, R960-25, 1:100) from Thermofisher. All antibodies have been previously published with citations available from the vendor and were validated for use via western blot indicating a protein band of the expected size.

10. Eukaryotic cell lines

a. State the source of each eukaryotic cell line used.	H1975, HCC827, and HCC4006 were from the American Type Culture Collection (ATCC). PC9 cells were a gift from Dr. F. Koizumi (National Cancer Center Research Institute and Shien-Lab, Tokyo, Japan).
b. Describe the method of cell line authentication used.	Cell line identity was confirmed by short-tandem repeat analysis (Genetica)
c. Report whether the cell lines were tested for mycoplasma contamination.	All cell lines used in this study tested negative for mycoplasma before their use.
d. If any of the cell lines used in the paper are listed in the database of commonly misidentified cell lines maintained by ICLAC, provide a scientific rationale for their use.	No commonly misidentified cell lines were used in this study.

Animals and human research participants

Policy information about studies involving animals; when reporting animal research, follow the ARRIVE guidelines

11. Description of research animals

Provide details on animals and/or animal-derived materials used in the study.	Female C.B-17 SCID mice were purchased from Taconic for both xenograft and PDX experiments and were between 4 and 8 weeks of age at the start of the experiment.

Policy information about studies involving human research participants

12. Description of human research participants

Describe the covariate-relevant population characteristics of the human research participants.	All patients were diagnosed with EGFR-mutant lung adenocarcinoma and treated with the indicated EGFR TKI. Analysis was blind to age and gender.